Structural Analysis of an Insect Lysozyme Exhibiting Catalytic Efficiency at Low Temperatures[†,‡]

Atsushi Matsuura,[§] Min Yao,[||] Tomoyasu Aizawa,[||] Nozomi Koganesawa,[||] Kazuo Masaki,[||] Mitsuhiro Miyazawa,[⊥] Makoto Demura,[||] Isao Tanaka,[||] Keiichi Kawano,*[,§] and Katsutoshi Nitta[||]

Faculty of Pharmaceutical Sciences, Toyama Medical and Pharmaceutical University, Toyama 930-0194, Japan, Graduate School of Science, Hokkaido University, Sapporo 060-0810, Japan, and National Institute of Agrobiological Science, Tsukuba, Ibaraki 305-8634, Japan

Received January 8, 2002; Revised Manuscript Received June 27, 2002

ABSTRACT: *Bombyx mori* lysozyme (*Bm*LZ), from the silkworm, is an insect lysozyme. *Bm*LZ has considerable activity at low temperatures and low activation energies compared with those of hen egg white lysozyme (HEWLZ), according to measurements of the temperature dependencies of relative activity (lytic and glycol chitin) and the estimation of activation energies using the Arrhenius equation. Being so active at low temperatures and low activation energies is characteristic of psychrophilic (cold-adapted) enzymes. The three-dimensional structure of *Bm*LZ has been determined by X-ray crystallography at 2.5 Å resolution. The core structure of *Bm*LZ is similar to that of *c*-type lysozymes. However, *Bm*LZ shows some distinct differences in the two exposed loops and the C-terminal region. A detailed comparison of *Bm*LZ and HEWLZ suggests structural rationalizations for the differences in the catalytic efficiency, stability, and mode of activity between these two lysozymes.

The immune system in insects consists of an arsenal of innate and inducible antibacterial factors (*1*, *2*), of which lysozyme is the most ubiquitous. Lysozyme catalyzes the hydrolysis of the β-1,4-glycosidic linkage between *N*-acetylglucosamine and muramic acid of the peptidoglycan, which is an important constituent of Gram-positive bacterial cell walls (*3*), with consequent lysis of the bacterial cell wall. In addition, the peptidoglycan fragments liberated during this hydrolysis elicit the inducible immune response in insects, e.g., the synthesis and secretion of antibacterial peptides and proteins such as cecropin (*4*, *5*).

Lysozyme is a basic protein that can act as a bactericide. It is widely distributed among vertebrate and invertebrate animals and has been utilized as a useful model protein for studying structural stability and folding mechanisms. Many researchers have investigated the features of vertebrate lysozymes (*6*−*10*). In contrast, although the amino acids and complementary DNA (cDNA) sequences of invertebrate lysozymes from several species have been determined, few of their physicochemical or structural properties have been analyzed.

The lysozyme-encoding gene has been isolated from *Bombyx mori*, and its expression system has been constructed (*11*−*13*). *Bm*LZ[1] has 119 amino acid residues, and its molecular weight is ∼13800. There is a deletion of 9 or 10 residues in comparison with the other vertebrate lysozymes, and the level of sequence identity between *Bm*LZ and HEWLZ is ∼40%. As this low level of sequence identity implies, vertebrate and invertebrate lysozymes are likely to be considerably different in their structural and functional features. Actually, while a typical lysozyme is a thermally very stable protein, low thermal stability has been reported in *Bm*LZ according to measurements made by differential scanning calorimetry (DSC) or circular dichroism (CD) spectroscopy (*12*). Additionally, according to the results of experiments on the typical hydrolytic pattern of a substrate, PNP-$(GlcNAc)_5$, the substrate-binding mode of *Bm*LZ is different from that of HEWLZ (*12*).

In this study, we analyzed the temperature dependence of the activity of *Bm*LZ and HEWLZ by measuring the lytic activity and glycol chitin activity, and we estimated the activation energies of these two lysozymes using the Arrhenius equation. To characterize the activities of *Bm*LZ, we determined its X-ray crystal structure by a molecular replacement method, refined at a resolution of 2.5 Å to an *R*-factor of 19.7% (R_{free} = 22.2%).

The psychrophilic (cold-adapted) enzyme is characterized by a high catalytic efficiency at low temperatures, accompanied by a low thermal stability. It has been proposed that psychrophilic enzymes such as psychrophilic α-amylase, β-lactamase, bacterial subtilisin, lipase, and trypsin have a more flexible molecular structure when compared to mesophilic and thermophilic counterparts, which allows them to compensate for the reduction of reaction rates at low temperatures, thus explaining the high specific activity of psychrophilic enzymes (*14*−*21*). The results of structural

[†] This work was supported by the Center of Excellence, Special Coordination Fund for Promoting Science and Technology, Science and Technology Agency, Japan, and the Program for Promotion of Basic Research Activities for Innovative Biosciences, Japan.

[‡] The coordinates have been submitted to the Protein Data Bank (entry 1GD6).

* To whom correspondence should be addressed.

[§] Toyama Medical and Pharmaceutical University.

[||] Hokkaido University.

[⊥] National Institute of Agrobiological Science.

[1] Abbreviations: *Bm*LZ, *B. mori* lysozyme; HEWLZ, hen egg white lysozyme; HLZ, human lysozyme; ASA, accessible surface area; GdnCl, guanidinium chloride.

10.1021/bi016099j CCC: $22.00
Published on Web 09/14/2002

analysis show similarity between *Bm*LZ and psychrophilic enzymes, thus explaining the effective activity at low temperatures and low thermal stability. For example, a small number of interdomain hydrogen bonds is one of the factors that reduce the stability of the cold trypsins (*21*). Furthermore, the difference in the substrate-binding mode between *Bm*LZ and HEWLZ can be understood by making a structural comparison of these two lysozymes.

MATERIALS AND METHODS

Materials. Expression and purification of *Bm*LZ were carried out using the expression system (continuous fermentation) of the methylotrophic yeast *Pichia pastoris* (*13*). The purity of the *Bm*LZ was confirmed with reverse-phase high-performance liquid chromatography (HPLC), sodium dodecyl sulfate−polyacrylamide gel electrophoresis (SDS−PAGE), and mass spectroscopy. HEWLZ was obtained from Seikagaku Kogyo (Tokyo, Japan).

Assay of Lysozyme Activity. We estimated the lytic activities of *Bm*LZ and HEWLZ against *Micrococcus lysodeikticus* using the turbidometric method (*22*) based on the decrease in turbidity of a 2.9 mL cell suspension (0.3 mg/mL) in 50 mM sodium phosphate buffer (pH 7.0) after the addition of 100 μL of a lysozyme solution (0.2 μM) in 50 mM sodium phosphate buffer (pH 7.0). The decrease in absorbance was monitored at 450 nm with a thermostatically controlled cell holder. The activities of both lysozymes against glycol chitin were determined as described previously (*23*, *24*) with slight modifications. First, 50 μL of 50 μM *Bm*LZ (2 μM HEWLZ) in a 0.1 M sodium chloride solution was added to 0.5 mL of a 0.5 mg/mL ethylene glycol chitin in 0.1 M sodium acetate buffer (pH 5.5) and incubated for 30 min. After the reaction, 1 mL of a potassium ferricyanide solution was added, and the reducing sugar was identified by incubation at 80 °C for 1 h. After the mixtures cooled, we read the optical density at 420 nm. Using these two methods, we measured the activity from 0 °C (glycol chitin activity) or 5 °C (lytic activity) to 65 °C at 5 °C increments. Maximal activity occurred at the optimal temperatures in *Bm*LZ (55 °C) and HEWLZ (60 °C). The relative activity of *Bm*LZ was represented at each temperature as a percentage of the maximal activity of *Bm*LZ at the optimal temperature, and that of HEWLZ reveals a percentage of the maximal activity of HEWLZ in the same way.

Crystallization, Data Collection, and Structure Refinement. The crystals of *Bm*LZ were obtained by vapor diffusion of hanging drops using 0.1 M sodium cacodylate buffer (pH 6.7) containing 10 mg/mL protein, 0.2 M ammonium sulfate, and 26% (w/v) PEG-8000 at 18 °C. After 2 weeks, the crystals had grown to a size of 0.3 mm × 0.2 mm × 0.2 mm. The space group of the crystal was $P4_12_12$ with the following cell dimensions: $a = b = 77.3$ Å and $c = 72.9$ Å. There is one monomeric molecule in an asymmetric unit ($V_M = 3.96$ Å^3/Da, solution content = 69.0%). The reflection data of the *Bm*LZ crystals were recorded on an imaging plate system, DIP-2000 (MAC Science), using Cu Kα (1.5418 Å) radiation at 10 °C. The data were integrated, scaled, and merged using the programs DENZO and SCALEPACK (*25*). The initial model of *Bm*LZ was obtained by molecular replacement using the program AMoRe (*26*), and the model was rebuilt with the program O (*27*). A search model was constructed from the atomic coordinates of HEWLZ (1LZA; *28*). The structural refinements were performed using the program CNS (*29*). Ten percent of the reflection data were set aside for the calculation of R_{free}.

Table 1: Absolute Activity Comparison

	*Bm*LZ	HEWLZ
Lytic Activity ($\times 10^9$ units/μmol)[a]		
15 °C	1.54	0.16
30 °C	3.04	0.76
55 °C (optimal temperature of *Bm*LZ)	4.18	2.05
60 °C (optimal temperature of HEWLZ)	4.15	2.07
Glycol Chitin Activity ($\times 10^3$ ΔA^{420}/μmol)		
15 °C	0.028	1.05
30 °C	0.043	2.07
55 °C (optimal temperature of *Bm*LZ)	0.090	5.98
60 °C (optimal temperature of HEWLZ)	0.087	6.29

[a] Units = ΔA^{450}/min/0.001. One unit is defined as the amount of enzyme able to decrease the OD at a rate of 0.001/min.

Analysis of Structural Features. The root-mean-square deviations (rmsds) were calculated with LSQKAB; the accessible surface area (ASA) was calculated with the programs SURFACE and RESAREA with a probe radius of 1.4 Å, and hydrogen bonds were analyzed with CONTAC using the following criteria: maximum distance of 3.5 Å from the donor to acceptor and minimal angles of 120° for O···H−N bonds and 90° for OH···O−C or NH···O−C bonds. LSQKAB, SURFACE, RESAREA, and CONTAC are contained in the CCP4 package (*30*). WHATIF (*31*) and O (*27*) were used for visual inspection of the structures.

Estimation of Protein Concentrations. The concentration of lysozymes was estimated by the absorbance at 280 nm using molar extinction coefficients for HEWLZ and *Bm*LZ at 280 nm of 38.5×10^3 and 27.9×10^3 cm^{-1} M^{-1}, respectively (*12*, *32*).

RESULTS AND DISCUSSION

Comparison of the Temperature Dependence of Catalytic Activity. We used two methods to determine the temperature dependencies of the activities and activation energies of *Bm*LZ and HEWLZ. The conventional method for measuring lytic activity has been to use the lysation of the cell wall of the Gram-positive bacterium known as *M. lysodeikticus*. Because this method measures the decrease in turbidity concomitant with cell lysation, the lytic activity does not directly reflect the catalytic reaction (the hydrolysis of the β-1,4-glycosidic linkage). Therefore, we also measured glycol chitin activity, because it could be measured directly by detecting the reducing groups produced by the catalytic reaction. Activities were represented as absolute or relative, that is, normalized against the activity at the optimal temperature. This was a convenient way to compare the activity−temperature profiles of HEWLZ and *Bm*LZ.

We measured the lytic activities of *Bm*LZ and HEWLZ against *M. lysodeikticus* at pH 6.0 and at several temperatures (from 5 to 65 °C, at 5 °C intervals). At 30 °C, the absolute activity of *Bm*LZ was found to be ∼4 times greater than that of HEWLZ (Table 1). The maximal activity occurs at the optimal temperature, and the optimal temperature of *Bm*LZ (55 °C) is slightly lower than that of HEWLZ (60 °C). The relative activity was represented at each temperature as a percentage of the maximal activity at the optimal

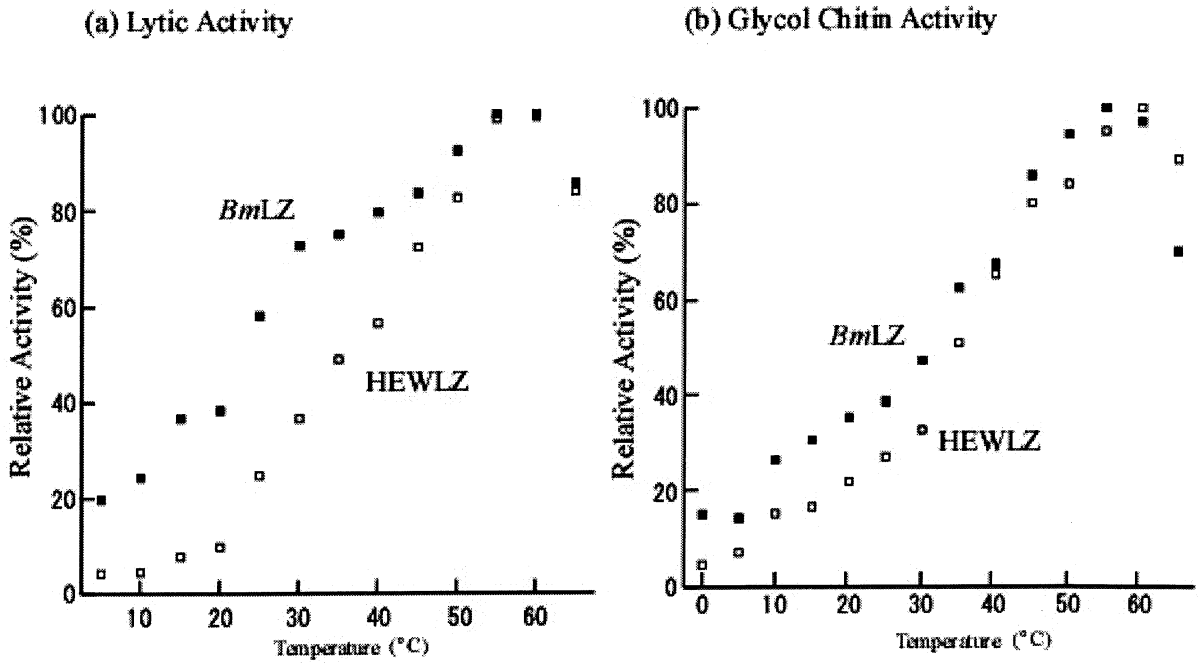

FIGURE 1: Temperature dependencies of the relative activity of *Bm*LZ and HEWLZ. The optimal temperatures of *Bm*LZ and HEWLZ are 55 and 66 °C, respectively. The relative activity was expressed at each temperature as a percentage of the activity at the optimal temperature: (a) lytic activity measurement and (b) glycol chitin activity measurement.

Table 2: Activation Energy Comparison

	lytic activity (kJ/mol)[a]	glycol chitin activity (kJ/mol)[a]
*Bm*LZ	26.6 ± 3.5	26.7 ± 1.8
HEWLZ	42.7 ± 6.2	52.3 ± 2.5

[a] Values ± standard deviations.

temperature. The temperature dependencies of the relative lytic activity of *Bm*LZ and HEWLZ are shown in Figure 1a. This figure shows that the relative activity of *Bm*LZ is higher than that of HEWLZ at low temperatures (at 15 °C, the relative activities of *Bm*LZ and HEWLZ are 37 and 8%, respectively).

We measured the glycol chitin activity of *Bm*LZ and HEWLZ at pH 5.5 and at several temperatures (from 0 to 65 °C, at 5 °C intervals). At 30 °C, the absolute activity of *Bm*LZ is ~50 times lower than that of HEWLZ, in contrast with the lytic activity (Table 1). As noted, the optimal temperature of *Bm*LZ (55 °C) is slightly lower than that of HEWLZ (60 °C). As was done with lytic activity, the relative glycol chitin activity was expressed at each temperature, and the temperature dependencies are shown in Figure 1b. This figure shows that the relative activity of *Bm*LZ is higher than that of HEWLZ at low temperatures (at 15 °C, the relative activities of *Bm*LZ and HEWLZ are 31 and 17%, respectively). These activity measurements show that *Bm*LZ has a lower optimal temperature and more effective activity at low temperatures than HEWLZ. These are the properties of psychrophilic enzymes.

Activation energy (E) was estimated by a least-squares fitting with a set of data points (relative activity k and temperature T) to the Arrhenius equation ($k = Ae^{-E/RT}$). The activation energy of *Bm*LZ is lower than that of HEWLZ, as listed in Table 2, which means that *Bm*LZ can catalyze at a lower activation energy than HEWLZ. The flexibility of protein molecules is reflected in perpetual conformation fluctuations. Linderström-Lang and Schellman noticed the existence and significance of this flexibility, and later the "fluctuation fit" concept of enzyme function was developed by Straub in 1964 with regard to conformational fluctuations. More flexible proteins require lower activation energies because conformational changes are necessary for the protein to reach the activation state.

Both the relative lytic and glycol chitin activities (k values) of *Bm*LZ are larger than those of HEWLZ over a low-temperature range (0−25 °C). This difference largely compensates for the reduction in the absolute reaction rates occurring at low temperatures. It has been proposed that this catalytic efficiency is gained by an appropriate folding flexibility (*33*). A loose conformation of the psychrophilic α-amylase is indeed suggested by the susceptibility of secondary structures to unfolding at moderate temperatures (*34*), by the fast denaturation rates induced by temperature, urea, or GdnCl, and by the shift of the optimal temperature of activity. Because the above proposition can be applied to *Bm*LZ, it is expected that *Bm*LZ is more flexible than HEWLZ, as would be the case for a psychrophilic enzyme.

X-ray Crystal Structure of BmLZ. The 2.5 Å resolution structure of *Bm*LZ was obtained by the molecular replacement (MR) method, refined to an R-factor of 19.7% (R_{free} = 22.2%). Table 3 shows the X-ray crystallographic parameters and refinement statistics. *Bm*LZ, as shown in Figure 2a, is composed of three major α-helices (helix A, residues Arg5−Lys14; helix B, residues Met22−Glu32; and helix C, residues Thr84−His97), two short helices (residues Ser76−Leu78 and Tyr103−Trp105), and an antiparallel β-sheet (S1, residues Thr40−Thr42; and S2, residues Lys48−Tyr50). The active site residues (Glu32 and Asp49) inside of a deep cleft are fully conserved, as is the case with other lysozymes.

Thermodynamic Parameters ΔC_p. To estimate the thermal stability of *Bm*LZ, the thermodynamic parameters [denaturation temperature (T_d), enthalpy change (ΔH), Gibbs free

Table 3: Statistics for the Final Collection Set and Refinement of X-ray Crystallography

data collection	
space group	$P4_12_12$
cell dimensions (Å)	$a = b = 77.27$, $c = 72.92$
resolution (Å)[a]	100−2.5 (2.59−2.5)
no. of observations	97639
$I/\sigma(I)$	20.90 (3.84)
total no. of unique reflections	7862 (747)
completeness (%)	98.6 (96.4)
multiplicity	7.12 (5.08)
R_{merge} (I)[b]	0.08 (0.30)
refinement	
resolution (Å)	10−2.5
R-factor (%)[c]	18.1
R_{free} (%)[d]	22.3
no. of non-hydrogen atoms	
protein atoms	963
water atoms	65
rms deviations from ideal geometry	
bond distances (Å)	0.009
bond angles (deg)	1.550
average B values (Å^2)	
all atoms	49.20
all protein atoms	38.85
main chain atoms	31.50

[a] Values in parentheses are for the automart resolution check. [b] $R_{merge} = \sum_h\sum_j|\langle I_h\rangle - I_{h,j}|/\sum_h\sum_j I_{h,j}$, where $\langle I_h\rangle$ is the mean intensity of symmetry equivalent reflections. [c] R-factor $= \sum|F_{obs} - F_{cal}|/\sum F_{obs}$, where F_{obs} and F_{cal} are the observed and calculated structure factors, respectively. [d] R_{free} was calculated for R-factor, using only an unrefined subset of reflection data (10%).

energy change (ΔG), and heat capacity change (ΔC_p)] for unfolding were obtained by Masaki et al. (*12*) by using differential scanning calorimetry (DSC). ΔC_p, which is thermodynamically equivalent to the slope of the plot of ΔH_{cal} versus T_d, is one of the most important parameters expressing the stability of globular proteins against unfolding. The respective values of ΔC_p are 1.07 (*Bm*LZ), 1.57 (HEWLZ), and 1.55 kcal mol^{-1} K^{-1} [human lysozyme (HLZ)] (*35*, *36*). Any increase in heat capacity induced by the unfolding of a globular protein is attributed to the exposure and hydration of internal amino acids during the unfolding process. Therefore, the thermal stability of the three enzymes can be estimated by comparing the amino acid compositions of the buried part of *Bm*LZ, HEWLZ, and HLZ.

ΔC_p between the arbitrary conformational states of a protein can be expressed as a linear combination of the differences in the solvent accessible surface areas in polar (ΔASA$_{pol}$) and apolar (ΔASA$_{ap}$) residues between those states, as follows:

$$\Delta C_p = \Delta C_{p,ap}{}^\circ\Delta\mathrm{ASA}_{ap} + \Delta C_{p,pol}{}^\circ\Delta\mathrm{ASA}_{pol}$$

where $\Delta C_{p,ap}{}^\circ$ and $\Delta C_{p,pol}{}^\circ$ are the elementary apolar and polar contributions to the total heat capacity increment, respectively. These ASA values were calculated using the program SURFACE (from the CCP4 program package) with a probe size of 1.4 Å. Water molecules in the folded structure were removed, and the cavity surface was included for the calculation of ΔASA. The ASA values of the unfolded state were taken as the sum of the areas of each residue in an extended Gly-X-Gly environment. The calculated values of ΔASA$_{pol}$, ΔASA$_{ap}$, and ΔC_p in *Bm*LZ, HEWLZ, and HLZ between the folded and unfolded states are listed in Table 4. The calculated values of ΔC_p correspond well with the

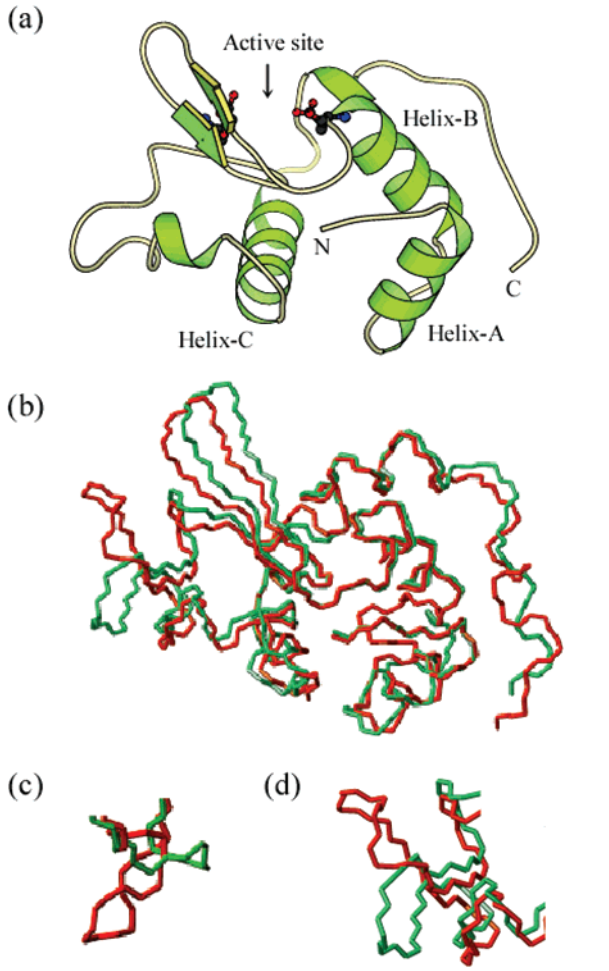

FIGURE 2: (a) Ribbon model of *Bm*LZ in which α-helices are sequentially labeled from A to C and catalytic residues are drawn (figure produced using MOLSCRIPT). (b−d) Superimposed main chain conformation of *Bm*LZ (green) and HEWLZ (orange). (b) Whole folding. (c) The region included loop 1. (d) The region included loop 2. This figure was produced using MOLMOL.

Table 4: ΔASAs of Apolar and Polar Residues and ΔC_p

	*Bm*LZ	HEWLZ	HLZ
ΔASA$_{ap}$ (Å^2)	6779.4	7524.9	7911.8
ΔASA$_{pol}$ (Å^2)	7114.7	7231.3	7460.4
calculated ΔC_p[a] (kcal K^{-1} mol^{-1})	1.201 ± 0.349	1.506 ± 0.367	1.620 ± 0.382
experimental ΔC_p (kcal K^{-1} mol^{-1})	1.07	1.57[b]	1.55

[a] $\Delta C_p = \Delta C_{p,ap}{}^\circ\Delta\mathrm{ASA}_{ap} + \Delta C_{p,pol}{}^\circ\Delta\mathrm{ASA}_{pol}$. $\Delta C_{p,ap}{}^\circ = 0.45 \pm 0.02$ cal K^{-1} mol^{-1} Å^{-2}. $\Delta C_{p,pol}{}^\circ = -0.26 \pm 0.03$ cal K^{-1} mol^{-1} Å^{-2}. [b] Pfeil and Privalov (*35*, *36*).

estimated values. The fact that the value of the thermodynamic parameter ΔC_p for *Bm*LZ is smaller than in two other lysozymes can be explained by the hydration of the residues during the disruption of the conformation.

Structural Basis for the Thermodynamic Stability and Flexibility. When the three-dimensional structure of *Bm*LZ is superimposed on HEWLZ in Figure 2b−d, the rmsd value for the main chain is 2.6 Å. This high rmsd value is due mainly to two loops, spanning residues Glu18−Leu21 (loop 1) and Lys63−Lys69 (loop 2) (corresponding to residues Asp18−Ser24 and Asp66−Asn74 in HEWLZ), with two or three residue deletions in each loop and the C-terminal region

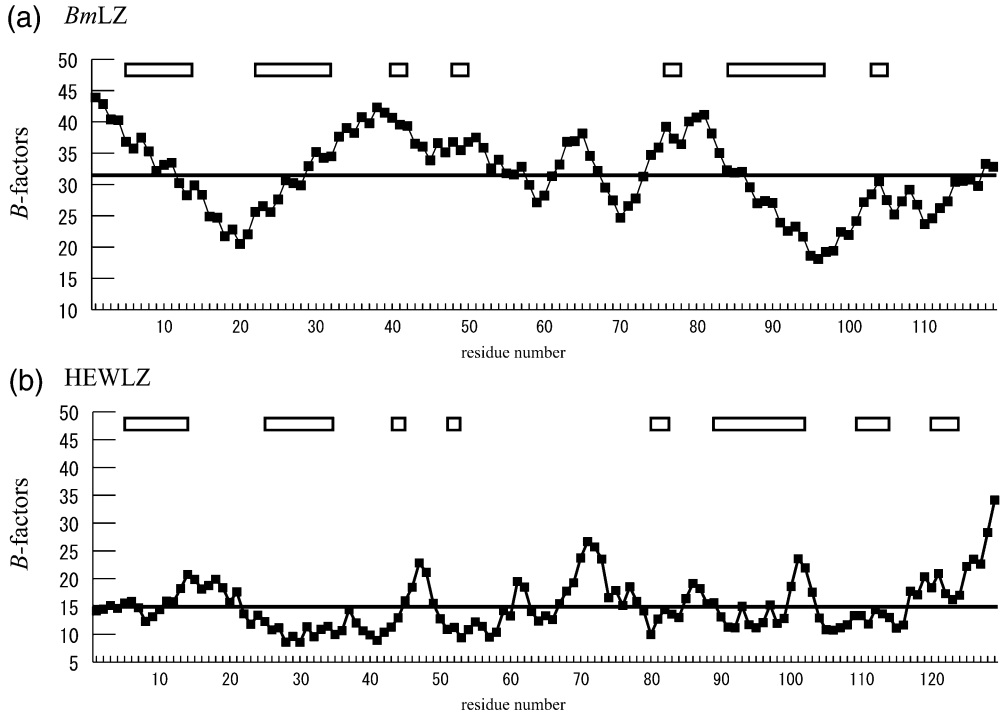

FIGURE 3: *B*-factor of main chain atoms (C_α) for (a) *Bm*LZ and (b) HEWLZ. The horizontal line shows the average *B*-factor.

Table 5: Lists of H-Bonds and Charge-Mediated Interactions around Loops 1 and 2

	*Bm*LZ	HEWLZ
around loop 1	His15 O−Lys91 NZ	His15 NE2−Thr89 OG1
	Arg23 NE−Pro114 O	His15 O−Lys96 NZ
	Asn24 OD1−Trp105 NE1	Leu17 O−Trp28 NE1
		Arg21 NE−Ser100 OG
		Arg21 NH2−Ser100 OG
		Tyr23 O−Trp28 NE1
		Tyr23 OH−Met105 N
		Asn27 OD1−Trp111 NE
around loop 2	Lys39 O−Gln54 NE2	Ala42 O−Gln57 NE2
	Asn43 OD1−Asp49 OD2	Asn44 ND2−Gln57 OE1
	Asn43 ND2−Asp49 OD2	Arg45 NH1−Arg68 NH1
	Ser47 OG−Asn56 ND2	Asn46 OD1−Asp52 OD1
	Lys48 N−Asp57 OD2	Asn46 OD1−Asn59 ND2
	Asp49 OD1−Asn56 ND2	Asp48 O−Arg61 NH2
	Tyr50 OH−Asp57 OD1	Asp48 OD2−Arg61 NE
	Tyr50 OH−Asp57 OD2	Ser50 OG−Asn59 ND2
	Asp57 O−Lys69 NZ	Thr51 N−Ser60 OG
	Arg58 O−Lys69 NZ	Thr51 OG1−Arg68 NH2
	Ser62 OG−Gly68 N	Asp52 OD1−Asn59 ND2
	Asp70 OD2−Lys92 NZ	Leu56 O−Trp108 NE1
		Ser60 OG−Thr69 OG1
		Trp63 O−Asn74 ND

Table 6: Comparison of Structural Parameters That Affect Thermostability or Enzymatic Activity between *Bm*LZ and HEWLZ

	*Bm*LZ	HEWLZ
no. of charged residues		
acidic	14	9
basic	21	17
no. of hydrophobic residues		
total	28	39
internal	9	10
aliphatic index	53.28	65.12
no. of H-bonds	154	188
H-bond/amino acid ratio	1.29	1.46
no. of salt bridges	8	3

of *Bm*LZ. The conformations of the loops in the enzymes of other species of vertebrates [human (1LZ1), canine (1QQY), equine (2EQL), turkey (135L), pheasant (1GHL), bobwhite quail (1DKJ), and rainbow trout (1LMN)] are similar to that of HEWLZ (*9*, *37*−*42*).

As a consequence of residue deletion, the networks of H-bonds and the charge-mediated interactions involving these loops are different in the two lysozymes, as shown in Table 5. Two hydrogen bonds in loop 1 in HEWLZ (Arg21−Ser100 and Tyr23−Met105), which help maintain the folding of the α-helix rich domain, are missing in *Bm*LZ. Similarly, three hydrogen bonds involving residues in loop 2 and in the β-sheet in HEWLZ (Arg45−Arg68, Thr51−Arg68, and Tyr53−Asp66) are absent in *Bm*LZ, and loop 2 is removed from the β-sheet. Thus, the stability around the β-sheet in *Bm*LZ is lower than that in HEWLZ.

The crystallographic temperature factors (*B*-factors) of *Bm*LZ also show the flexibility of this β-sheet. Plots of the *B*-factor of the main chain atoms of *Bm*LZ and HEWLZ are shown in Figure 3. Although the *B*-factor of the β-sheet in HEWLZ is remarkably lower than the average *B*-factor, this region of *Bm*LZ has a *B*-factor much higher than the average, which indicates that the conformation of the β-sheet of *Bm*LZ is flexible. There is a catalytic residue (Asp49) in the β-sheet region, so the flexibility of this region probably contributes to the effective activity at low temperatures and to the low activation energy of *Bm*LZ.

A comparison between the total number of hydrogen bonds present in each enzyme also supports the finding of a higher degree of flexibility of *Bm*LZ (Table 6). There are 154 hydrogen bonds in *Bm*LZ and 188 in HEWLZ (water-mediated hydrogen bonds are not included), with the H-bond/amino acid ratio having a value of 1.29 in *Bm*LZ and 1.46 in HEWLZ.

One additional factor that contributes to the lower thermal stability and increased flexibility of *Bm*LZ is the fact that the last Leu113−Ile116 C-terminal residues are in an

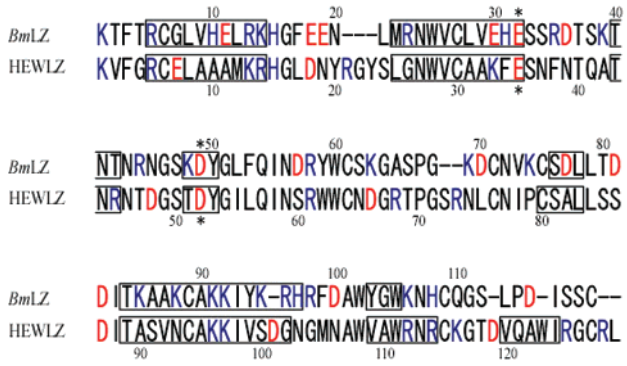

FIGURE 4: Sequence alignment of *Bm*LZ and HEWLZ. Asterisks (*) denote catalytic residues. Boxed regions show where the residues formed secondary structures. Positively and negatively charged residues are shown in blue and red, respectively.

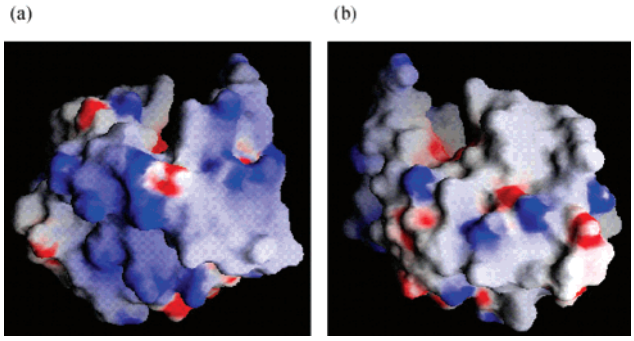

FIGURE 5: Electrostatic potential at the surface of *Bm*LZ. The surface of *Bm*LZ is a bipolarized, positive charge-rich surface (a) and a non-positive charge-rich surface (b). These surfaces are 180° opposite each other. Positively and negatively charged residues are shown in blue and red, respectively.

extended conformation, and no α-helix structure (as observed in HEWLZ) is present.

Protein Structure and Catalytic Activity. As shown in Figure 4, the amino acid sequence of *Bm*LZ reveals a low level of identity (44% residue) and similarity (58% residue, G = A = S, S = T, V = L = I, F = W = Y, E = D = R = K, and Q = N) with that of HEWLZ. *Bm*LZ has more charged residues than HEWLZ does, as shown in Table 6. Furthermore, most of the charged residues of *Bm*LZ are located on the outside of the molecule, and the distribution of positive charges has a tendency toward bipolarity (Figure 5). It seems reasonable to suppose that the frequency with which the lysozyme contacts the cell wall of the bacterium is related to the level of lytic activity. Compared to that of HEWLZ, the surface of *Bm*LZ is more highly charged, and its distribution of charges is polarized. Thus, on the surface of *Bm*LZ there is a positively charged side that can contact favorably the negatively charged cell wall of a Gram-positive bacterium. This explains why the absolute lytic activity of *Bm*LZ is higher than that of HEWLZ, as shown by the experimental results (Table 1).

On the other hand, in terms of absolute glycol chitin (simple substrate) activity, *Bm*LZ exhibited activity remarkably lower than HEWLZ ($\sim^1/_{10}$ as much) (Table 1). This may be due to the different substrate-binding mode of *Bm*LZ as compared with that of HEWLZ. Typical lysozymes, such as HEWLZ, bind to six consecutive sugar rings in a cleft known as subsites A−F. The cleavage site (Asp52 and Glu35) for HEWLZ is located between subsites D and E (*43*), and the cleavage site (Asp49 and Glu32) for *Bm*LZ is conformationally identical with that for HEWLZ. The experiments using a substrate, PNP-$(GlcNAc)_5$, revealed that the hydrolytic patterns of substrates for *Bm*LZ and HEWLZ were apparently different (*12*). Although both A−E and B−F binding modes were observed in HEWLZ, the B−F binding mode was obviously dominant in *Bm*LZ. It is possible that subsite A is not included in the binding site of *Bm*LZ. The crystal structures of the substrate-binding sites of *Bm*LZ and HEWLZ are described in Figure 6, and as the figure shows, the binding of a substrate to subsite A in *Bm*LZ may be inhibited by the salt bridge between Asp70 and Arg96. At the same time, Asp101 (HEWLZ) is missing from *Bm*LZ, and so is the interaction between its side chain and the nitrogen atom at position 2 of GlcNAc.

Conclusion. Two kinds of activity measurements showed that *Bm*LZ has a lower optimal temperature of activity and greater relative activity at low temperatures than HEWLZ. In addition, the activation energy of *Bm*LZ is lower than that of HEWLZ in accordance with the flexibility of *Bm*LZ. The three-dimensional structure of *Bm*LZ was determined by X-ray crystallography, and the observed differences with the structure of HEWLZ help explain the flexibility of *Bm*LZ. These results make clear the correlation among the activity, flexibility, and thermal stability in proteins that catalyze under different circumstances. Furthermore, the difference in the substrate-binding mode between *Bm*LZ and HEWLZ is explained by the structural comparison of these two lysozymes.

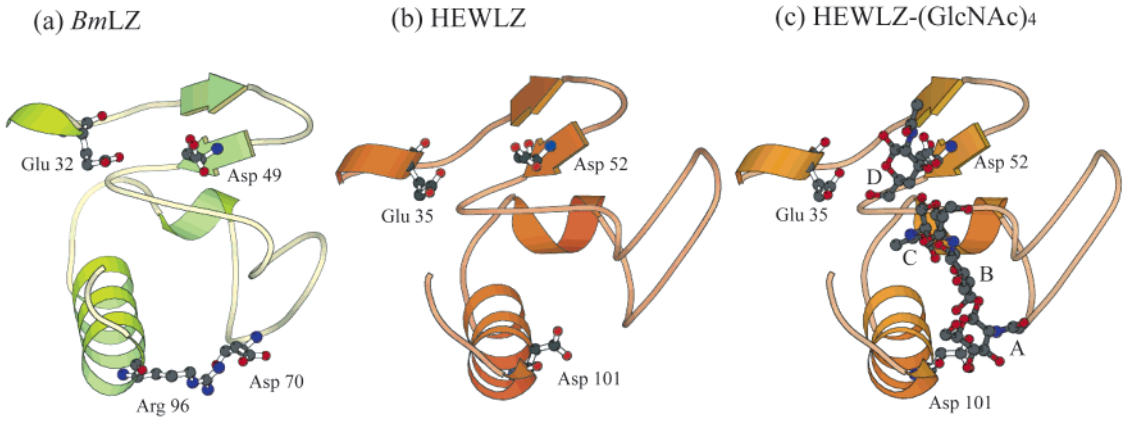

FIGURE 6: Substrate-binding sites (subsites A−D). (a) *Bm*LZ, (b) HEWLZ, and (c) HEWLZ with $(GlcNAc)_4$. This figure was produced using MOLSCRIPT.

ACKNOWLEDGMENT

We thank Prof. Tadashi Ueda of the Graduate School of Pharmaceutical Sciences, Kyushu University (Fukuoka, Japan), for kind advice regarding the measurement of glycol chitin activity.

SUPPORTING INFORMATION AVAILABLE

Lytic and glycol chitin activity measurements. This material is available free of charge via the Internet at http://pubs.acs.org.

REFERENCES

1. Boman, H. G. (1991) *Cell 65*, 205−207.
2. Hultmark, D. (1993) *Trends Genet. 9*, 178−183.
3. Prager, E. M., and Jollès, P. (1996) in *Lysozymes: Model Enzymes in Biochemistry and Biology* (Jollès, P., Ed.) pp 9−31, Birkhäuser Verlag, Basel, Switzerland.
4. Morishima, I., Horiba, T., and Yamano, Y. (1994) *Comp. Biochem. Physiol., Part A: Mol. Integr. Physiol. 108*, 311−314.
5. Morishima, I., Horiba, T., Iketani, M., Nishioka, E., and Yamano, Y. (1995) *Dev. Comp. Immunol. 19*, 357−363.
6. Strynadka, N. C. J., and James, M. N. G. (1996) in *Lysozymes: Model Enzymes in Biochemistry and Biology* (Jollès, P., Ed.) pp 185−222, Birkhäuser Verlag, Basel, Switzerland.
7. McKenzie, H. A., and White, F. H., Jr. (1991) *Adv. Protein Chem. 41*, 174−315.
8. Mizuguchi, M., Masaki, K., and Nitta, K. (1999) *J. Mol. Biol. 292*, 1137−1148.
9. Koshiba, T., Yao, M., Kobashigawa, Y., Demura, M., Nakagawa, A., Tanaka, I., Kuwajima, K., and Nitta, K. (2000) *Biochemistry 39*, 3247−3257.
10. Sasahara, K., and Nitta, K. (1999) *Protein Sci. 8*, 1469−1474.
11. Lee, W., and Brey, P. T. (1995) *Gene 161*, 199−203.
12. Masaki, K., Aizawa, T., Koganesawa, N., Nimori, T., Bando, H., Kawano, K., and Nitta, K. (2001) *J. Protein Chem. 20*, 107−113.
13. Koganesawa, N., Aizawa, T., Masaki, K., Matsuura, A., Nimori, T., Bando, H., Kawano, K., and Nitta, K. (2001) *Protein Eng. 14*, 705−710.
14. Feller, G., Narinx, E., Arpigny, J. L., Aittaleb, M., Baise, E., Genicot, S., and Gerday, C. (1996) *FEMS Microbiol. Rev. 18*, 189−202.
15. Feller, G., Zekhnini, Z., Lamotte-Brasseur, J., and Gerday, C. (1997) *Eur. J. Biochem. 244*, 186−191.
16. Feller, G., d'Amico, D., and Gerday, C. (1999) *Biochemistry 38*, 4613−4619.
17. Gerday, C., Aittaleb, M., Arpigny, J. L., Baise, E., Chessa, J. P., Garsoux, G., Petrescu, I., and Feller, G. (1997) *Biochim. Biophys. Acta 1342*, 119−131.
18. Gerday, C., Aittaleb, M., Bentahir, M., Chessa, J. P., Claverie, P., Collins, T., D'Amico, S., Dumont, J., Garsoux, G., Georlette, D., Hoyoux, A., Lonhienne, T., Meuwins, M. A., and Feller, G. (2000) *Trends Biotechnol. 18*, 103−107.
19. Jaenicke, R. (1991) *Eur. J. Biochem. 202*, 715−728.
20. Davail, S., Feller, G., Narinx, E., and Gerday, C. (1994) *J. Biol. Chem. 269*, 17448−17453.
21. Schrøder, H. K., Willassen, N. P., and Smals, A. O. (2000) *Eur. J. Biochem. 267*, 1039−1049.
22. Yoshimura, K., Toibana, A., Kikuchi, K., Kobayashi, M., Hayakawa, T., Nakahama, K., Kikuchi, M., and Ikehara, M. (1987) *Biochem. Biophys. Res. Commun. 145*, 712−718.
23. Yamada, H., and Imoto, T. (1981) *Carbohydr. Res. 92*, 160−162.
24. Ito, Y., Yamada, H., Nakamura, M., Yoshikawa, A., Ueda, T., and Imoto, T. (1993) *Eur. J. Biochem. 213*, 649−658.
25. Otwinowski, Z. (1993) in *Data Collection and Processing: Proceedings of the CCP4 Study Weekend* (Sawyer, L., Isaacs, N., and Bailey, S., Eds.) pp 56−62, Daresbury Laboratory, Warrington, U.K.
26. Navaza, J. (1994) *Acta Crystallogr. A50*, 157−163.
27. Jones, T. A., Zou, J. Y., Cowan, S. W., and Kjeldgaard, M. (1991) *Acta Crystallogr. A47*, 110−119.
28. Maenaka, K., Matsushima, M., Song, H., Sunada, F., Watanabe, K., and Kumagai, I. (1995) *J. Mol. Biol. 247*, 281−293.
29. Brünger, A. T., Adams, P. D., Clore, G. M., Delano, W. L., Gros, P., Grosse-Kunstleve, R. W., Jiang, J. S., Kuszewski, J., Nilges, M., Pannu, N. S., Read, R. J., Rice, L. M., Simonson, T., and Warren, G. L. (1998) *Acta Crystallogr. D54*, 905−921.
30. Collaborative Computational Project Number 4 (1994) *Acta Crystallogr. D50*, 760−763.
31. Vriend, G. (1990) *J. Mol. Graphics 8*, 52−56.
32. Takahashi, T., Hamaguchi, K., Hayashi, K., Imoto, T., and Funatsu, M. (1965) *J. Biochem. (Tokyo) 58*, 385−387.
33. Hochachka, P. W., and Somero, G. N. (1984) *Biochemical adaptations*, Princeton University Press, Princeton, NJ.
34. Feller, G., Lonhienne, T., Deroanne, C., Libioulle, C., Van Beeumen, J., and Gerday, C. (1992) *J. Biol. Chem. 267*, 5217−5221.
35. Pfeil, W., and Privalov, P. L. (1976) *Biophys. Chem. 4*, 23−32.
36. Pfeil, W., and Privalov, P. L. (1976) *Biophys. Chem. 4*, 33−40.
37. Artymiuk, P. J., and Blake, C. C. (1981) *J. Mol. Biol. 152*, 737−762.
38. Tsuge, H., Ago, H., Noma, M., Nitta, K., Sugai, S., and Miyano, M. (1992) *J. Biochem. (Tokyo) 111*, 141−143.
39. Harata, K., Abe, Y., and Muraki, M. (1998) *Proteins 30*, 232−243.
40. Lescar, J., Souchon, H., and Alzari, P. M. (1994) *Protein Sci. 3*, 788−798.
41. Chacko, S., Silverton, E. W., Smith-Gill, S. J., Davies, D. R., Shick, K. A., Xavier, K. A., Willson, R. C., Jeffrey, P. D., Chang, C. Y., Sieker, L. C., and Sheriff, S. (1996) *Proteins 26*, 55−65.
42. Karlsen, S., Eliassen, B. E., Hansen, L. K., Larsen, R. L., Riise, B. W., Smalas, A. O., Hough, E., and Grinde, B. (1995) *Acta Crystallogr. D51*, 354−367.
43. Kumagai, I., Maenaka, K., Sunada, F., Takeda, S., and Miura, K. (1993) *Eur. J. Biochem. 212*, 151−156.

BI016099J